J Therm Anal Calorim (2010) 99:191–195
DOI 10.1007/s10973-009-0148-7

Effects of gaseous hydrogenation on crystallization behavior of melt-spun $Mg_{63}Pr_{15}Ni_{22}$ amorphous ribbons

Y. L. Du · W. Li · Y. H. Deng · F. Xu

Received: 14 January 2009 / Accepted: 7 April 2009 / Published online: 19 June 2009

Abstract Effects of gaseous hydrogenation on crystallization behavior of melt-spun $Mg_{63}Pr_{15}Ni_{22}$ amorphous ribbons have been investigated. The crystallization peak temperature T_{p1} shifted to higher temperature with increasing heating rate for the un-hydrogenated $Mg_{63}Ni_{22}Pr_{15}$ metallic glass, however, it is nearly unchanged for the hydrogenated sample. The present work indicates that the crystallization is a nucleation-and-growth process for the un-hydrogenated $Mg_{63}Ni_{22}Pr_{15}$ metallic glass. However, the crystallization of hydrogenated sample begins with nucleation and then diffusion-controlled growth takes place.

Keywords Amorphous ribbons · Crystallization · Hydrogenation

Introduction

Metallic glasses offer some attractive structural, physical and chemical properties, which make them suitable for various technological applications [1–3]. Among the amorphous alloys, Mg-based metallic glasses are of high interest because of their high strength to weight ratio and relatively low price [4–6]. Recently, a new Mg-Ni-Pr metallic glass was easily prepared in air atmosphere [7]. The unusual high manufacturability and high oxygen resistance of this Mg-based metallic glass will contribute a lot to its application in industry. However, to promote its practical utilization, we need to know more about this fascinating Mg-based metallic glass. The interaction of hydrogen with the amorphous microstructure is a fundamental issue in metallic glasses [8, 9]. It is known that many metallic glasses contain elements that can absorb hydrogen. In addition, there are large amounts of atomic-scale open volumes in metallic glasses. Thus, it is reasonable that hydrogen shows high solubility and diffusivity in metallic glasses. It was reported that hydrogen could strongly influence the properties of metallic glasses even at small concentrations. For example, the hydrogen embrittlement behavior of various Fe-, Co- and Zr-based amorphous alloys has been reported [10–12]. And hydrogenation also has a strong effect on the thermal stability of metallic glasses [13, 14].

For Mg-based metallic glasses [15, 16], it is more important to study the interaction between hydrogen and the amorphous alloys because Mg element has a high affinity with hydrogen. In our previous work, a dramatic enhancement of thermal stability induced by hydrogenation was found in amorphous $Mg_{63}Ni_{22}Pr_{15}$ metallic ribbons, which has not ever been found in other metallic glasses [17]. Crystallization behavior is a fundamental field of metallic glasses. Thermal analysis has been extensively used for studying the crystallization behavior of metallic glasses [18–20]. In the present work, the hydrogenation effect on crystallization behavior of amorphous $Mg_{63}Ni_{22}Pr_{15}$ metallic ribbons was studied by differential scanning calorimetry (DSC). Non-isothermal and isothermal kinetic analyses were performed and the mechanism was discussed.

Y. L. Du (✉) · W. Li · Y. H. Deng · F. Xu
Department of Materials Science and Engineering,
Nanjing University of Science and Technology,
210094 Nanjing, China
e-mail: yldu_njust@mail.njust.edu.cn

Experimental

$Mg_{63}Ni_{22}Pr_{15}$ alloy ingot was prepared by vacuum induction levitation melting on water-cooled copper crucible under Ar atmosphere. Melt-spun ribbons were produced by the single-roller melt-spinning technique. The amorphous $Mg_{63}Ni_{22}Pr_{15}$ ribbons were ground and then hydrogen was introduced into the powders by a conventional Sieverts-type system. After three activation cycles of full charge and discharge, gaseous hydrogenation was carried out under hydrogen pressure of 3.4 MPa at 313 K. The hydrogen content in the amorphous powders was measured to be 0.38 wt%. Thermal stability of the un-hydrogenated and hydrogenated samples was examined by differential scanning calorimetry (DSC) in Ar atmosphere using a Netzsch STA449C instrument. Non-isothermal DSC curves were measured with selected heating scan rates of 5, 10, 20 and 40 K/min. Isothermal DSC curves were obtained with selected temperatures of 463, 468, 473, 478 K for the un-hydrogenated samples, and 560, 563, 568 K for the hydrogenated samples, respectively.

Results and discussion

To investigate the kinetics of glass transition and crystallization behaviors, DSC measurements of the as-quenched $Mg_{63}Ni_{22}Pr_{15}$ ribbons were carried out at the heating rates of 5, 10, 20 and 40 K/min. As shown in Fig. 1, each DSC trace exhibits a distinct glass transition, a wide undercooled liquid region, and exothermic peaks due to crystallization of the glassy phase. The glass transition temperature T_g, the onset crystallization temperature T_x, and the crystallization peak temperature T_{p1} are all shifted to higher temperature with increasing heating rate, which indicates that both the glass transition and the crystallization behave in a markedly kinetic nature [21]. It should be noted that the second crystallization peak is more sensitive to the heating rate and almost disappears at a high heating rate of 40 K/min, which indicates that this crystallization process has a low critical heating rate to avoid nucleation and growth. Similar behavior was previously observed in $Zr_{41}Ti_{14}Cu_{12.5}Ni_{10}Be_{22.5}$ amorphous alloy [13, 14].

Figure 2 shows the isothermal DSC curves for the un-hydrogenated $Mg_{63}Ni_{22}Pr_{15}$ amorphous alloy at annealing temperatures of 463, 468, 473 and 478 K, where the corresponding incubation time τ were worked out to be 13.9, 5.53, 2.4 and 1.05 min, respectively. Each trace shows a single high symmetrical exothermic peak. The peak shifts to longer times for the lower annealing temperature. These results clearly indicate that the crystallization is a nucleation-and-growth process [22]. It is known that the isothermal DSC

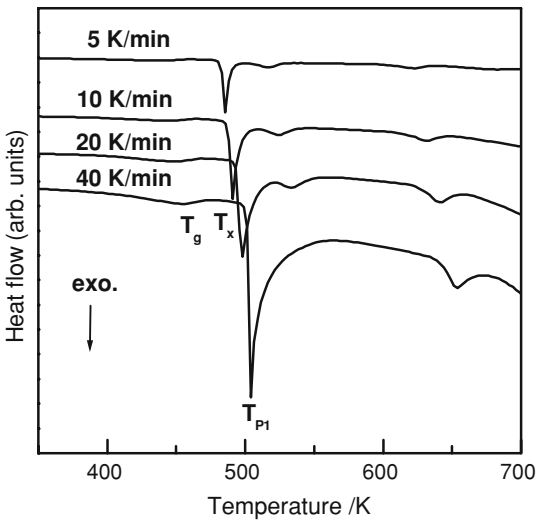

Fig. 1 DSC curves for the un-hydrogenated $Mg_{63}Ni_{22}Pr_{15}$ metallic glass at different heating rates

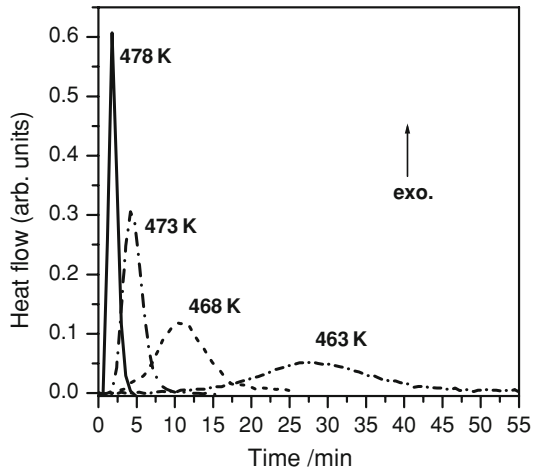

Fig. 2 Isothermal DSC curves for the un-hydrogenated $Mg_{63}Ni_{22}Pr_{15}$ metallic glass at annealing temperatures of 463 K, 468 K, 473 K and 478 K, where the incubation times have been excluded

traces can be analyzed by the Johnson–Mehl–Avrami (JMA) equation [23]:

$$\ln\left[-\ln\left(1-x_c\right)\right] = \ln\left(k\right) + n\ln\left(t-\tau\right) \quad (1)$$

where x_c is the crystallized volume fraction, t the annealing time, τ the incubation time, n the Avrami exponent related to the dimensionality of nucleation and growth, and k a kinetic constant of the process. Here, the fraction of crystallization is assumed to be proportional to the heat release. The behavior of x_c as a function of t is shown in Fig. 3. It can be seen that the shape of the curves is typical "S" type. The Avrami exponent n was determined to be 2.8 for annealing at 478 and 473 K, and 2.9 for annealing at 468 and 463 K, which means that crystallization starts from

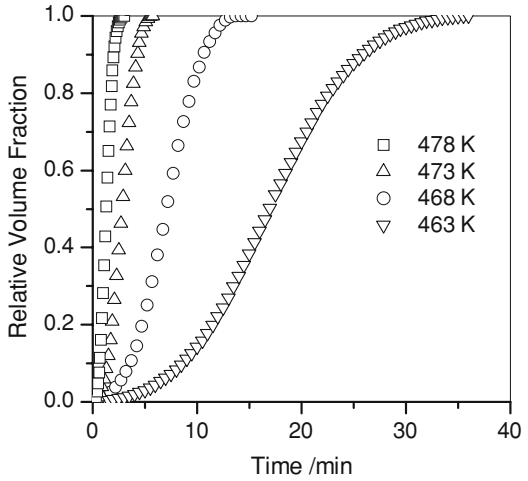

Fig. 3 Relative volume fractions of the crystallization component as a function of time at different isothermal annealing temperatures for the un-hydrogenated $Mg_{63}Ni_{22}Pr_{15}$ metallic glass, where the incubation times have been excluded

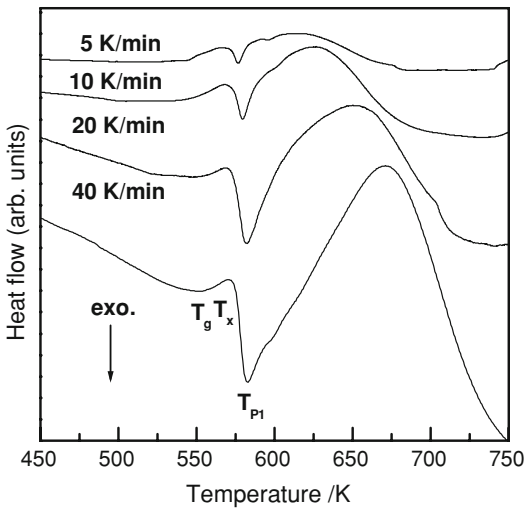

Fig. 4 DSC curves for the hydrogenated $Mg_{63}Ni_{22}Pr_{15}$ metallic glass at different heating rates

crystalline grains of small dimensions with an increasing nucleation rate [24].

Figure 4 shows the DSC curves of the hydrogenated $Mg_{63}Ni_{22}Pr_{15}$ metallic glass at different heating rates. The hydrogenation effects on the crystallization behavior are obvious in the hydrogenated sample. As shown in the figure, the glass transition temperature, the onset crystallization temperature, and the crystallization temperature of the hydrogenated $Mg_{63}Ni_{22}Pr_{15}$ metallic glass are 550, 570 and 577 K measured at heating rate of 20 K/min, much higher than the corresponding values of 440, 470 and 499 K for the un-hydrogenated sample. This means that dramatic enhancement of thermal stability occurs in $Mg_{63}Ni_{22}Pr_{15}$ metallic glass due to hydrogenation. Comparing with the un-hydrogenated sample, it can be seen that the crystallization peak temperature T_{p1} are near unchanged with increasing the heat rates for the hydrogenated sample. In addition, the second crystallization peak only can be detected at the heating rate of 5 K/min. Another interesting feature is the broad endothermic peak corresponding to the desorption of hydrogen from the hydrogenated sample. The desorption of hydrogen shows a strong kinetic nature. As shown in the figure, as the heating rate is increased, the desorption peak shifts to higher temperature and the corresponding peak flux becomes higher.

Figure 5 shows the isothermal DSC curves for the hydrogenated $Mg_{63}Ni_{22}Pr_{15}$ ribbons at annealing temperatures of 560, 563, and 568 K, respectively. A strong effect of hydrogenation on the isothermal crystallization is found. As shown in the figure, only very weak exothermic peaks were detected for the hydrogenated samples. On the whole, the calorimetric signal continuously decreases until reaching a saturation at long times of annealing. This

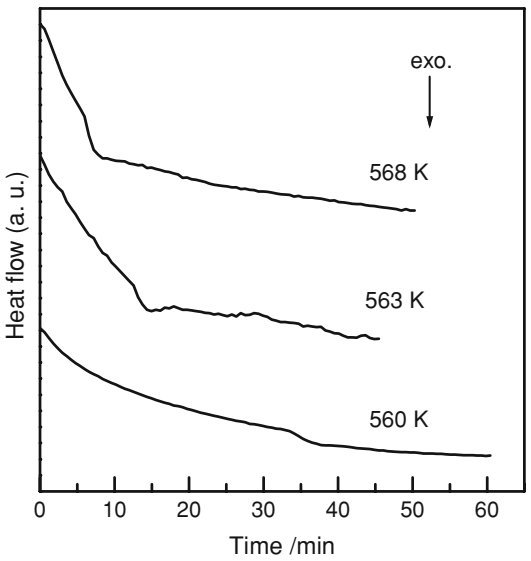

Fig. 5 Isothermal DSC curves for the hydrogenated $Mg_{63}Ni_{22}Pr_{15}$ metallic glass at annealing temperatures of 560 K, 563 K, and 568 K

indicates that after very fast nucleation leading to the formation of a high initial density of nuclei, diffusion-controlled growth takes place [25].

The effects of hydrogenation on the crystallization process were also studied by XRD. As shown in Fig. 6, the XRD pattern for the as-spun sample shows only a broad peak indicating the amorphous structure in the as-spun state. After hydrogenated, the amorphous structure was retained as reported in our previous work [17]. The as-spun and hydrogenated amorphous samples were then annealed at 538 and 638 K respectively, which is higher than the peak temperature for the primary crystallization. After the

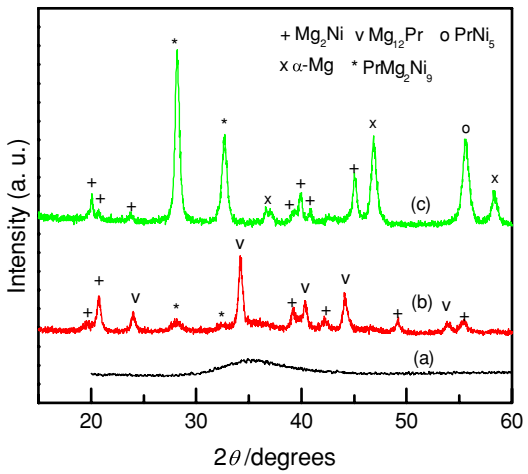

Fig. 6 XRD patterns of the (*a*) as-spun sample, (*b*) as-spun sample annealed at 538 K for 20 min, (*c*) hydrogenated sample annealed at 638 K for 20 min

annealing, $Mg_{12}Pr$, Mg_2Ni and $PrMg_2Ni_9$ phases can be detected for the as-spun samples. A strong effect of hydrogenation on the crystallization behavior was observed. As can be seen from Fig. 6, the phases after the primary crystallization were Mg_2Ni, α-Mg, $PrMg_2Ni_9$ and $PrNi_5$.

It is known that the crystallization of metallic glasses is related to the atomic rearrangement at short-range order [26]. Large concentration fluctuations of several alloy components are required before crystallization begins. Considering the strong interaction of hydrogen with Mg and Pr atoms in $Mg_{63}Ni_{22}Pr_{15}$ amorphous alloy which exhibit strong metal hydride formation tendencies, the rearrangement of atoms become more difficult during the crystallization of the glassy alloy.As a result,the crystallization temperature increased and the thermal stability enhanced. It was reported that the thermal stability of a Zr-based metallic glasses was enhanced slightly by hydrogenation [13, 14]. In the present work, the dramatic enhancement of thermal stability of $Mg_{63}Ni_{22}Pr_{15}$ metallic glasses can be attributed to the high affinity of Mg, Pr atoms and hydrogen. In the same way, the rearrangement of atoms during the crystallization process can be hindered by the introduction of hydrogen, which leads to the appearance of different phases after crystallization.

Conclusions

The crystallization behaviors of $Mg_{63}Ni_{22}Pr_{15}$ metallic glasses are strong influenced by hydrogenation. The analysis of the isothermal crystallization kinetics indicates that the crystallization is a nucleation-and-growth process for the un-hydrogenated $Mg_{63}Ni_{22}Pr_{15}$ metallic glass, however, the crystallization of hydrogenated sample begins with nucleation and then diffusion-controlled growth takes place. The rearrangement of atoms during the crystallization process can be hindered by the introduction of hydrogen, which leads to the changes of the crystallization behaviors.

Acknowledgments This work is supported by the Natural Science Foundation of Jiangsu Province (BK2007213), the Young Scholar Foundation of Nanjing University of Science and Technology (Njust200404), and "Qinglan Project" Foundation of Jiangsu Province.

References

1. Inoue A. Stabilization of metallic supercooled liquid and bulk amorphous alloys. Acta Mater. 2000;48:279–306.
2. Johnson WL. Bulk glass-forming metallic alloys: science and technology. MRS Bull. 1999;24:42–56.
3. Wang WH, Dong C, Shek CH. Bulk metallic glasses. Mater Sci Eng R. 2004;44:45–89.
4. Inoue A, Kato A, Zhang T, Kim SG, Masumoto T. Mg-Cu-Y amorphous-alloys with high mechanical strengths produced by a metallic mold casting method. Mater Trans JIM. 1991;32:609–16.
5. Ma H, Xu J, Ma E. Mg-based bulk metallic glass composites with plasticity and highstrength. Appl Phys Lett. 2003;83:2793–5.
6. Jang JSC, Ciou JY, Hung TH, Huang JC, Du XH. Enhanced mechanical performance of Mg metallic glass with porous Mo particles. Appl Phys Lett. 2008;92:011930.
7. Wei YX, Xi XK, Zhao DQ, Pan MX, Wang WH. Formation of MgNiPr bulk metallic glasses in air. Mater Lett. 2005;59:945–7.
8. Guo X, Ma L, Inoue A. Improved hydrogen storage capacity of $Ti_{60}Zr_{15}Ni_{15}Cu_{10}$ amorphous alloy. Mater Trans. 2001;42:2133–5.
9. Spassov T, Rangelova V. Hydriding properties of amorphous Ni-B alloy studied by DSC and thermogravimetry. Thermochim Acta. 1999;326:69–73.
10. Nagumo M, Takanashi T. Hydrogen embrittlement of some Fe-base amorphous alloys. Mater Sci Eng A. 1976;23:257–9.
11. Misra RDK, Aktar D. Hydrogen embrittlement behavior of a cobalt-based amorphous alloy. Mater Lett. 1985;3:500–2.
12. Jayalakshmi S, Kim KB, Fleury E. Effect of hydrogenation on the structural, therma and mechanical properties of Zr-50-Ni-27-Nb-18-Co-5 amorphous alloy. J Alloys Compd. 2006;417:195–202.
13. Peng DL, Yan M, Sun JF, Shen J, Chen YY, McCartney DG. Enhanced thermal stability by pre-charged hydrogen of a Zr-based bulk metallic glass. J Alloys Compd. 2005;400:197–201.
14. Suh D, Dauskardt RH. Effects of pre-charged hydrogen on the mechanical and thermal behavior of Zr-Ti-Ni-Cu-Be bulk metallic glass alloys. Mater Trans. 2001;42:638–41.
15. Spassov T, Köster U. Hydrogenation of amorphous and nanocrystalline Mg-based alloys. J Alloys Compd. 1999;287:243–50.
16. Yamaura SI, Kim HY, Kimura H, Inoue A, Arata Y. Thermal stabilities and discharge capacities of melt-spun Mg–Ni-based amorphous alloys. J Alloys Compd. 2002;339:230–5.
17. Du YL, Deng YH, Xu F, Chen G, Chen GL. Gaseous hydrogenation and its effect on thermal stability of $Mg_{63}Ni_{22}Pr_{15}$ metallic glass. Chin Phys Lett. 2006;23:3320–2.
18. Revesz A. Crystallization kinetics and thermal stability of an amorphous $Fe_{77}C_5B_4A_{12}GaP_9Si_2$ bulk metallic glass. J Therm Anal Calorim. 2008;91:879–84.

19. Pratap A, Rao TLS, Lad KN, Dhurandhar HD. Isoconversional vs. model fitting methods—a case study of crystallization kinetics of a Fe-based metallic glass. J Therm Anal Calorim. 2007;89:399–405.
20. Simon P, Illekova E, Mojumdar SC. Kinetics of crystallization of metallic glasses studied by non-isothermal and isothermal DSC. J Therm Anal Calorim. 2006;83:67–9.
21. Liu L, Wu ZF, Chen L. A kinetic study of the non-isothermal crystallization of a Zr-based bulk metallic glass. Chin Phys Lett. 2002;19:1483–6.
22. Pratap A, Raval KG, Gupta A, Kulkarni SK. Nucleation and growth of a multicomponent metallic glass. Bull Mater Sci. 2000;23:185–8.
23. Johnson MA, Mehl RF. Reaction kinetics in processes of nucleation and growth. Trans Am Inst Min Metall Pet Eng. 1939;135:416–58.
24. Xu F, Du YL, Gao P, Han ZD, Chen G, Wang SQ, et al. Crystallization of melt-spun $Mg_{63}Ni_{22}Pr_{15}$ amorphous alloy ribbon. J Alloys Compd. 2007;441:76–80.
25. Spassov T, Solsona P, Surinach S, Baro MD. Nanocrystallization in $Mg_{83}Ni_{17-x}Y_x$ ($x = 0$, 7.5) amorphous alloys. J Alloys Compd. 2002;345:123–9.
26. Mattern N, Kühn U, Ehrenberg H, Neuefeind J, Eckert J. Short-range order of $Zr_{62-x}Ti_xAl_{10}Cu_{20}Ni_8$ bulk metallic glasses. Acta Mater. 2002;50:305–14.